ACS SyntheticBiology

pubs.acs.org/synthbio Letter

Conditional Protein Rescue by Binding-Induced Protective Shielding

Andrew S. Gaynor and Wilfred Chen*

Cite This: ACS Synth. Biol. 2020, 9, 2639−2647 Read Online

ACCESS | Metrics & More | Article Recommendations | Supporting Information

ABSTRACT: Synthetic protein-level circuits offer an extra layer of cellular control on top of conventional gene-level circuits. Here, we describe a technology that allows conditional protein rescue (CPR) from proteasomal degradation using different protein inputs as masking agents. A target protein is fused to a degron tag and an affinity sensor domain. The use of nanobodies as the sensor domain offers a generalizable strategy to execute a wide range of protein-level circuits with ease. The utility of this new strategy was successfully demonstrated to distinguish cancer cells out of a healthy population using the HPV-specific E7 protein as a cellular marker. Because CPR can be programmed to execute more complex Boolean logic designs using cell-specific proteomes, this platform offers a highly modular and scalable framework for a wide range of applications based on synthetic protein circuits.

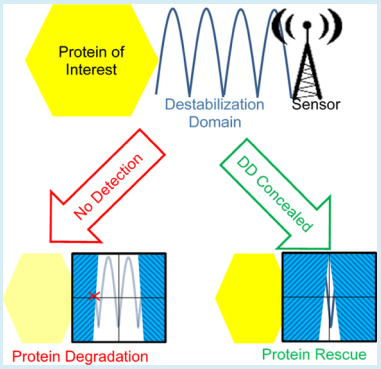

KEYWORDS: *cancer, prodrugs, protein engineering, protein−protein interactions, synthetic biology*

Conditional control of protein levels remains elusive for many biological applications. RNA interference (RNAi) destroys mRNA, but it can frequently be off-target or partially potent.[1] While small molecule-responsive transcriptional switches are frequently used to regulate mRNA levels, the overall dynamic is limited by the half-life of the target protein.[2−4] Another common method is the fusion of a degradation domain (DD) to a protein of interest (POI),[5] which drastically reduces its half-life and allows faster fluctuations in the intracellular level.[6,7] As we recently reviewed,[8] while several approaches can modulate protein degradation in response to a small molecule,[9−11] they do not allow protein concentration control in response to native cellular environments. Ideally, a modular platform that combines rapid protein turnover by DDs with temporal and autonomous responsiveness to cellular environments will greatly expand our ability to generalize the strategy for conditional protein rescue (CPR) in a wide range of biological contexts.

Coordinated degradation of cyclins is a key mechanism to ensure correct progression through the cell cycle.[12−14] This exquisite control between accumulation and depletion of cyclins is tightly regulated by changes in cellular protein information, suggesting a possible framework for CPR. One potential strategy is based on the Ac/N-End Rule pathway used for protein quality control, which recognizes and targets certain Nα-terminally acetylated residues for degradation.[15−17] Remarkably, the same acetylated residue is also necessary for proper interaction with cellular chaperones, which sterically shield the degradation domain and preserve properly folded proteins. The ability to shield the DD from initiating degradation has inspired the design of a new generation of artificial protein stability switches for conditional degradation.[18] A concealed DD between two proteins was only activated upon release by protease cleavage.[19,20] While this report represents a first step toward CPR, it is unable to couple endogenous cellular cues to modulate degradation.

We sought to implement CPR by using cellular protein cues to provide masking and unmasking of DDs. In this design, a small sensor domain is appended to the DD. When a binding target is present, the DD is effectively concealed, and the target protein is rescued (Figure 1a). We demonstrated that effective CPR can be executed using both covalent SpyTag/SpyCatcher conjugation and noncovalent nanobody/antigen interaction. Selective rescue of the yeast cytosine deaminase using this strategy enabled strong prodrug activation and targeted cell killing. The flexibility in choosing different masking targets provides a straightforward method to generalize the strategy for conditional protein rescue in a wide range of biological contexts, including oncoprotein detection.

RESULTS AND DISCUSSION

To evaluate the feasibility of CPR, we first utilized the SpyCatcher (SC) and SpyTag (ST) system, which provides the most stable *in vivo* interaction because of covalent conjugation.[21] A well-characterized synthetic cODC1-like C-

Received: July 9, 2020
Published: October 7, 2020

https://dx.doi.org/10.1021/acssynbio.0c00367
ACS Synth. Biol. 2020, 9, 2639−2647

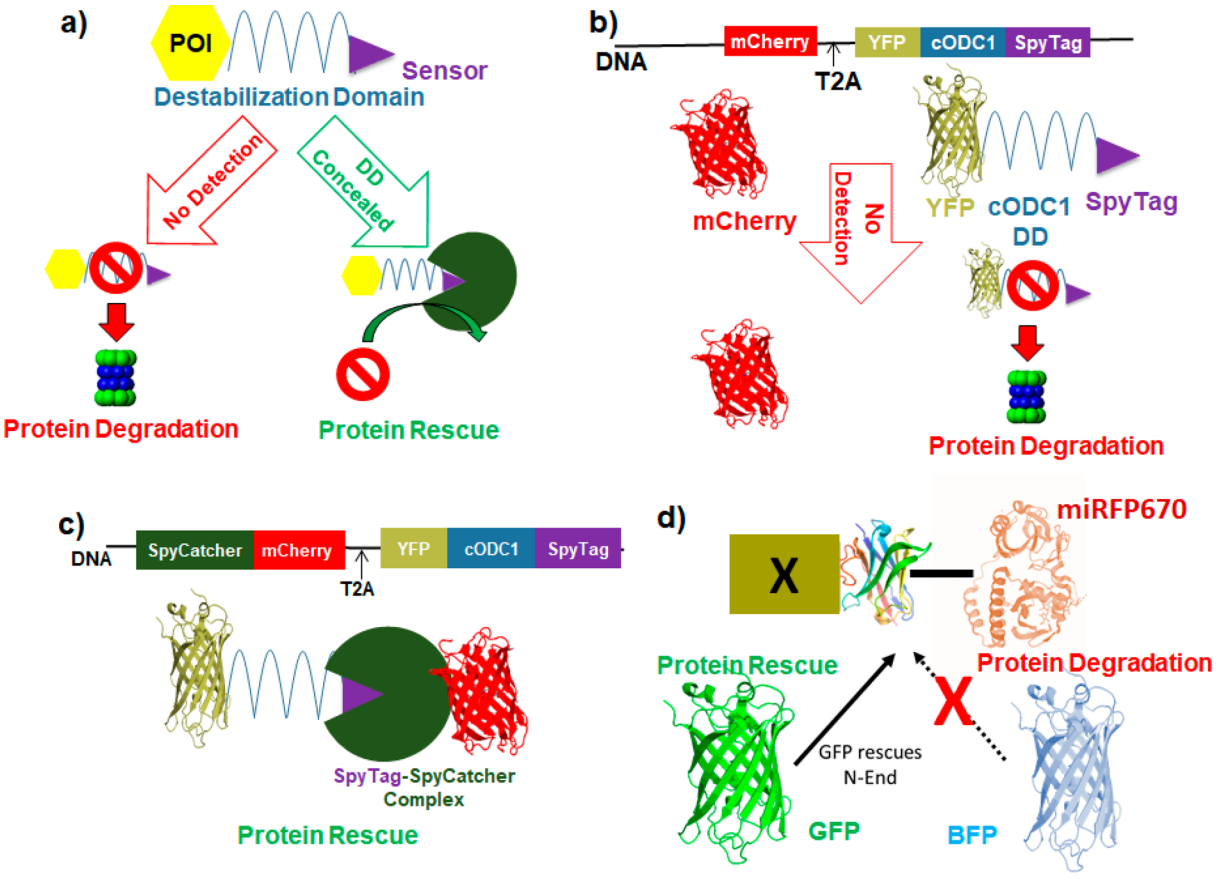

Figure 1. Conditional protein rescue (CPR) via masking the DD. (a) The DD (blue squiggle) contains a small sensor domain (purple triangle) fused to its C-terminus. In the absence of the corresponding binding target to the sensor, the POI (yellow hexagon) is recruited to the proteasome via DD interaction (red symbol) and degradation proceeds (left). Interaction with the target (green cut-out circle) conceals the DD from the proteasomal recruitment, and the POI is rescued from degradation (right). (b) CPR via the C-terminus cODC1 DD. YFP is fused to the cODC1 DD and SpyTag (sensor) and coexpressed with mCherry as a transfection marker. YFP is degraded by proteasome recognition of cODC1, and mCherry remains. (c) When mCherry is fused to the SpyCatcher (target), the SpyTag sensor recruits SpyCatcher-mCherry, sterically concealing cODC1 and rescuing YFP by CPR. (d) CPR via the N-end rule DD. A far-red fluorescent protein, miRFP670, can be rescued by steric shielding the N-end rule residue through the noncovalent interaction between the nanobody GBP1 and its antigen, GBP. BFP, which is not recognized by GBP1, does not induce rescue.

degron tag was used as the DD with kinetics that allow for rescue to occur.[18] By fusing the DD-ST to a fluorescent reporter, we generated YFP-cODC1-ST, an unstable complex that can be rescued by SC. We employed mCherry as an orthogonal transfection reporter (Figure 1b). Both the YFP fusion and mCherry were expressed under one promotor by use of a polycistronic viral T2A self-cleaving sequence.[22,23] To induce rescue of YFP, SC was fused to mCherry for easy tracking (Figure 1c).

To evaluate the rescue efficiency, HeLa cells were transfected with SC-mCherry:T2A:YFP-cODC1-ST or the control, mCherry:T2A:YFP-cODC1-ST, without SC. Expression of both proteins was tracked by fluorescent microscopy and Western blot over 60 h. Western blot analysis (Figure 2a) demonstrated that mCherry was detected consistently in both constructs roughly 15 h post-transfection. YFP gradually disappeared in cells expressing only mCherry, while a strong band corresponding only to the ligated YFP products was detected for cells expressing SC-mCherry. The absence of any unligated YFP with SC-mCherry coexpression highlights that ligation between ST and SC is solely responsible for YFP rescue due to shielding of the DD (Figure 2a). This is further supported by the fluorescent images (Figure S1) demonstrating efficient YFP rescue due to DD shielding by ST-SC ligation.

To quantify CPR more accurately, miRFP670, a near-infrared, monomeric, fluorescent protein with a completely orthogonal signal to YFP on the flow cytometer,[24] was used to generate SC-miRFP670:T2A:YFP-cODC1-ST and the negative control, SH3-miRFP670:T2A:YFP-cODC1-ST, where SH3 is a well-known Src homology 3 (SH3) domain and does not interact with ST.[25,26] Flow cytometry showed that CPR rescue increased throughout the entire time course, with roughly 7.5-fold increase in the YFP signal after 60 h (Figure 2b). Western blots confirmed the covalent conjugation between SC and ST but not SH3 and ST, as expected (Figure S2).

In order to adapt this technology toward more relevant cellular targets, a small, monomeric sensor capable of noncovalent interaction with endogenous proteins is required. Camel single-domain antibody fragments or nanobodies, are ideal because of their small size (~13 kDa) and the ability to generate high-affinity nanobodies for many protein targets.[27,28] An anti-GFP nanobody (GBP1, $k_D \sim 1$ nM) was first fused to the C-terminus of an miRFP670-cODC1 fusion (Figure 3a).[29] Unlike conjugation of a SC-fusion onto an adjacent ST to

https://dx.doi.org/10.1021/acssynbio.0c00367
ACS Synth. Biol. 2020, 9, 2639−2647

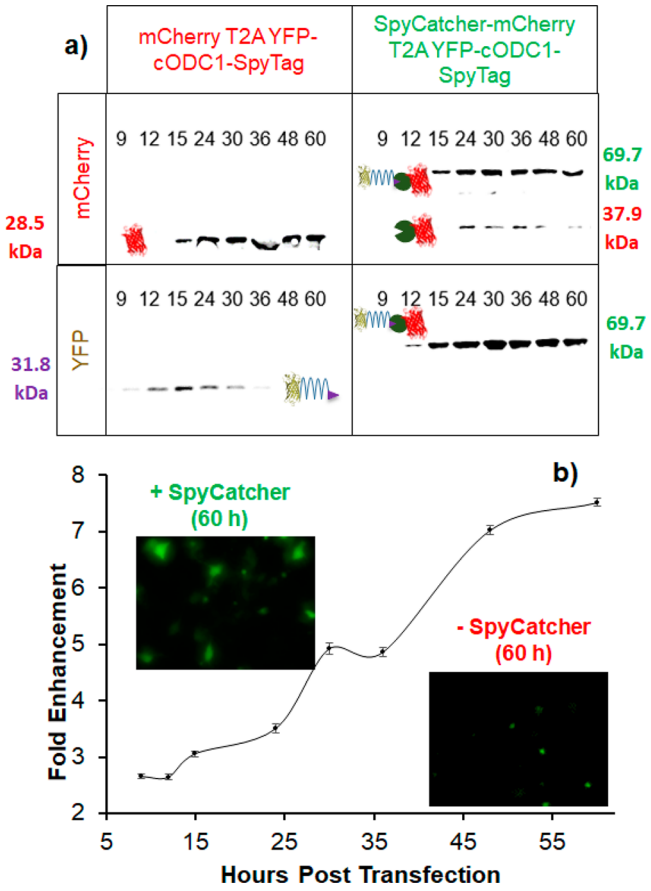

Figure 2. YFP rescue from cODC1-mediated degradation via SpyTag-SpyCatcher interaction. (a) Western blotting of HeLa cell lysate. Expression of YFP and mCherry/mCherry-SpyCatcher were detected by their respective antibodies at the hours post-transfected indicated in the figure for each lane. The upward shift in the protein size for the mCherry-SpyCatcher samples was the result of SpyTag-SpyCatcher conjugation. Protein sizes are included for each blot. (b) Flow cytometry quantification of YFP enhancement by CPR. miRFP670, a near-infrared fluorescent protein with a completely orthogonal signal to YFP on the flow cytometer, was used in place of mCherry. Fold enhancement is YFP signal normalized to miRFP670 expression in the SpyCatcher-miRFP670 fusion sample relative to the control with no SpyCatcher expression. A line is included through the data points to help visualize the upward trend. Inset images are representative of 60 h post-transfection to show relative levels of GFP rescue. Error bars represent 95% confidence intervals.

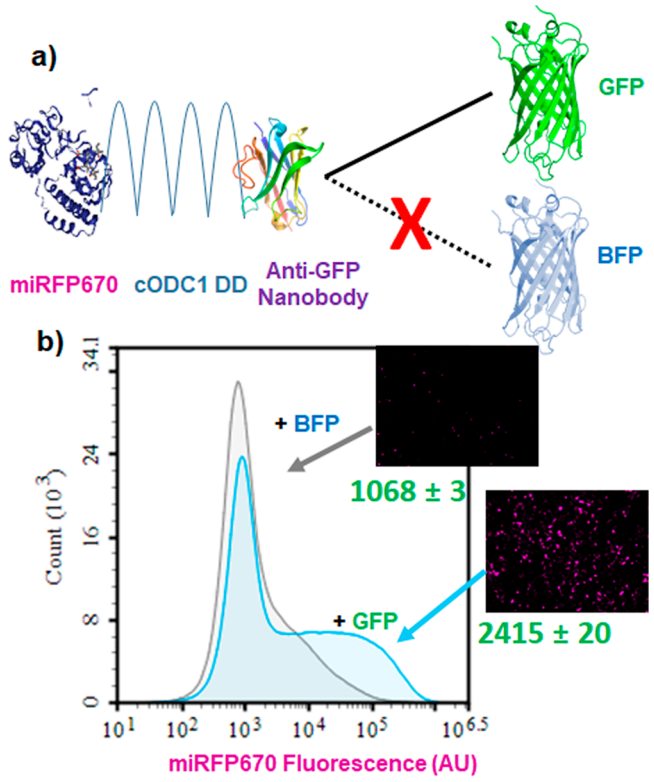

Figure 3. Rescuing a POI using noncovalent nanobody-antigen interactions. (a) miRFP670 is fused to the cODC1 DD and an anti-GFP nanobody (GBP1), which still maintains its inherently unstable feature. HeLa cells expressing miRFP670-cODC1-GBP1 were cotransfected with either BFP or GFP for CPR. Coexpression with BFP alone did not result in miRFP670 rescue due to a lack of interaction with GBP1, while coexpression with GFP restored miRFP670 signal due to DD masking. (b) Flow cytometry analysis of miRFP670 fluorescence in the presence of BFP (gray) and GFP (blue) after 48 h. The corresponding median whole-cell fluorescent values are included. Inserts show fluorescent microscopy images of miRFP670 for each sample.

cOCD1, no masking of the DD was observed as virtually no miRFP670 signal was detected (Figure 3b). This is somewhat unexpected as a small structural nanobody was physically tethered next to the DD. We speculate that the steric masking of the DD may be size dependent. To test this hypothesis, we fused a larger maltose-binding protein (MBP; 43 kDa) to GBP1. This resulted in improved miRFP670 signal (Figure S3), consistent with the proposed enhanced DD masking and miRFP670 rescue.

After establishing that a small nanobody GBP1 can be fused after the DD without impacting degradation, we next investigated whether protein rescue could be attained based on GBP1 and GFP interaction. In the presence of BFP, which could not associate with GBP1, miRFP670 was still efficiently degraded. In contrast, expression of GFP efficiency rescued miRFP670 from degradation due to GFP shielding of the DD (Figure 3b and Figure S3). These results provide the feasibility to repurpose nanobody−antigen interactions to elicit CPR for many different synthetic biology applications of practical interest.

Yeast cytosine deaminase (yCD) is a prodrug-converting enzyme (PCE) that transforms the innocuous 5-fluorocytosine (5-FC) into the cytotoxic 5-fluorouracil (5-FU), and it has been used successfully for the treatment of glioblastoma.[30,31] To adapt CPR for prodrug targeting, we generated yCD-cODC1-GBP1 to exploit yCD as the POI to test how well this strategy can control 5-FC activation. GFP again served as a visually trackable surrogate for a cancer-relevant protein, while BFP was used as a negative control to mimic the absence of a cancer-relevant protein surrogate. The ability to trigger cell death by 5-FU was used to indicate the overall efficiency. As expected, 5-FU killed large quantities of cells regardless of GFP, while cell viability was high when no drugs were administered (Figure 4a). When treated with 5-FC, only cells coexpressing GFP were killed in similar quantities to those being treated directly with 5-FU (Figure 4b).

Although the degree of cell killing in the absence of GFP but with 5-FC is slightly higher than cells without 5-FC addition (Figure 4b), this undesired outcome can be rectified by using a stronger degradation signal (*e.g.*, UbL) or a combination of

https://dx.doi.org/10.1021/acssynbio.0c00367
ACS Synth. Biol. 2020, 9, 2639−2647

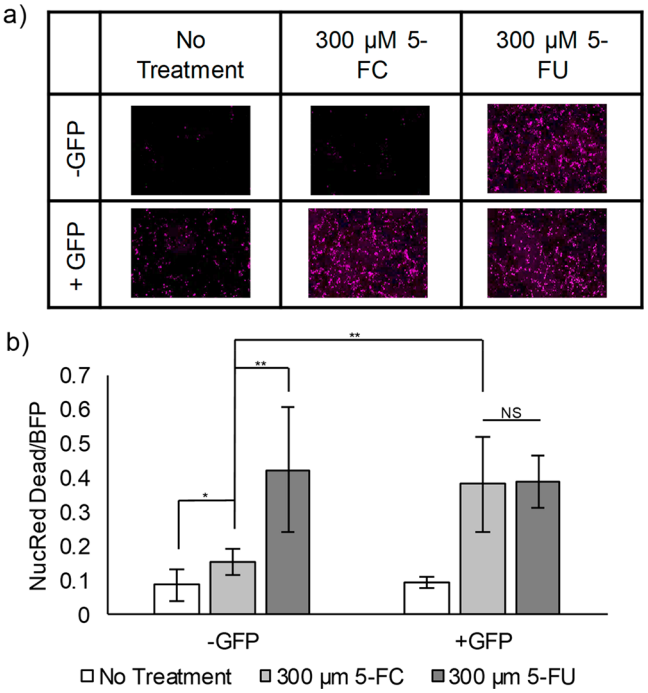

Figure 4. Controlling yCD activity via protein-nanobody interaction-mediated rescue. (a) Fluorescent images of a cell death dye. Presence of the dye (pink) indicates a dead cell. Cells die in large numbers in the presence of 5-FU. Cells are killed by 5-FC, the prodrug, only when GFP rescues yCD by stabilizing the DD-nanobody fusion. (b) Quantification of all fluorescent images, normalizing NucRed Dead dye to BFP, the protein transfection marker. Cells were transfected and either treated with no drugs (No Treatment), 5-FC, or 5-FU (n = 10; * = p < 0.05; ** = p < 0.01; NS = no statistical significant difference).

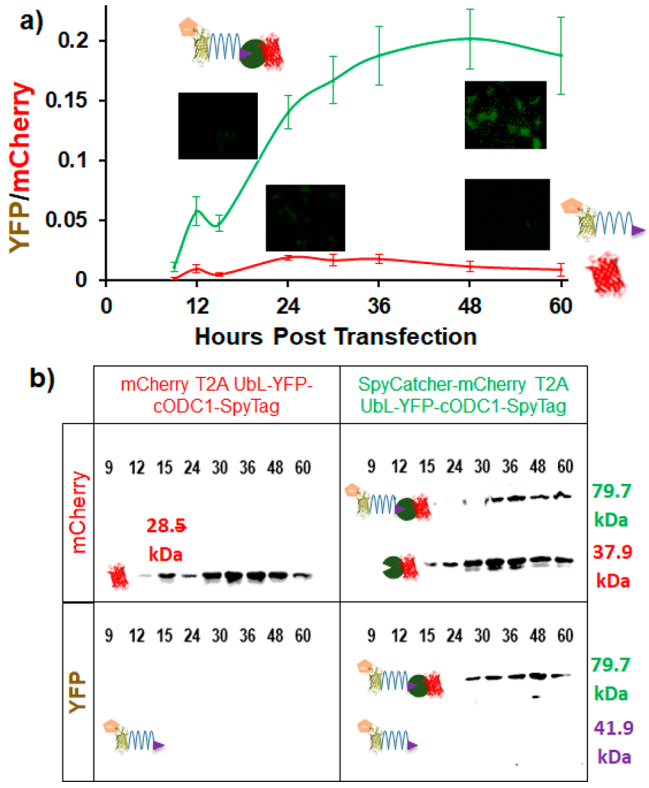

Figure 5. Tuning YFP rescue using the stronger proteasome binding UbL domain (orange pentagon) to improve degradation kinetics. a) Quantification of fluorescent microscopy measuring YFP intensity normalized by mCherry intensity. Compared to designs without UbL (see Figure S5), background YFP intensity was decreased (red line), but the ability of YFP to be rescued decreased as well (green line). The images show HeLa cells with the YFP signal (green) 9 and 60 h post-transfection. Error bars represent ±95% confidence interval (n = 5). (b) Western blotting of HeLa cell lysate. The UbL domain is effective in eliminating any detectable traces of YFP expression without rescue (lower left box). Coexpression with SpyCatcher rescued YFP from degradation (lower right box). Protein sizes are included for each blot.

multiple DDs. Previously, it was reported that an unstructured domain and a proteasomal targeting moiety are both necessary for efficient proteasomal degradation.[32] To determine if our CPR design could block access to the unstructured cOCD1 domain in the presence of a second proteasomal-targeting moiety, we fused one copy of the ubiquitin-like (UbL) domain to the N-terminus of YFP.[33] UbL has been shown to target its fusion partners directly to the proteasome more effectively than the cODC1 tag alone.[34,35] The combination of UbL and cODC1 DD enhanced YFP degradation as neither fluorescent microscopy (Figure 5a and Figure S4) nor Western blot (Figure 5b) could detect YFP in the absence of SpyCatcher-mCherry. Coexpression of SpyCatcher-mCherry was again able to rescue YFP, although the rescued YFP level was lower than without the UbL domain (Figure S5). The increase in protein degradation kinetics competes more aggressively with the SpyTag-SpyCatcher reaction, resulting in less rescue. This result highlights the modularity of our approach in adjusting signal background and rescue intensity.

Encouraged by the CPR results using the cOCD1 C-degron, we next turned to the N-end rule protein degradation pathway. Because the N-end rule substrates are recognized by specific binding proteins known as N-recognins, which deliver these substrates to the 26S proteasome for destruction,[36,37] chaperones are able to protect their targets via steric interference.[16] We reasoned that expressing a sensing nanobody directly following a destabilizing N-terminus residue as a fusion to a POI should result in rescue when the corresponding nanobody's target is coexpressed (Figure 1d).

To perform CPR using an N-end rule degron, we added an ubiquitin (Ub) domain to the N-terminus of a POI, which is subsequently cleaved by an endogenous deubiquitylase, exposing the desired N-terminus residue for destabilization.[38] We generated three Ub:X-GBP1-miRFP670 fusions, where X is either methionine (M, half-life = 30 h), leucine (L, half-life = 5.5 h), or arginine (R, half-life = 1.0 h).[39] These constructs were coexpressed with either BFP or GFP. Coexpression of BFP resulted in weak miRFP670 fluorescence scaling to the reported half-lives (Figure S6). Coexpressing with GFP resulted in the rescue of miRFP670 in all three cases (Figure 6a and Figure S7). Due to its extremely low background yet high level of rescue, an Arg N-terminus degron elicited an unprecedented >50-fold increase in protein fluorescence. To ensure that CPR was not a phenomenon specific to GBP1 and GFP-mediated rescue, we replaced GBP1 with LaM4, a nanobody that detects mCherry.[40] For all constructs, only coexpression with mCherry resulted in higher EGFP fluorescence (Figure S8). To illustrate the broader applicability of our CPR approach toward native protein targets, we next extended our design to detect human papillomavirus (HPV)-

https://dx.doi.org/10.1021/acssynbio.0c00367
ACS Synth. Biol. 2020, 9, 2639−2647

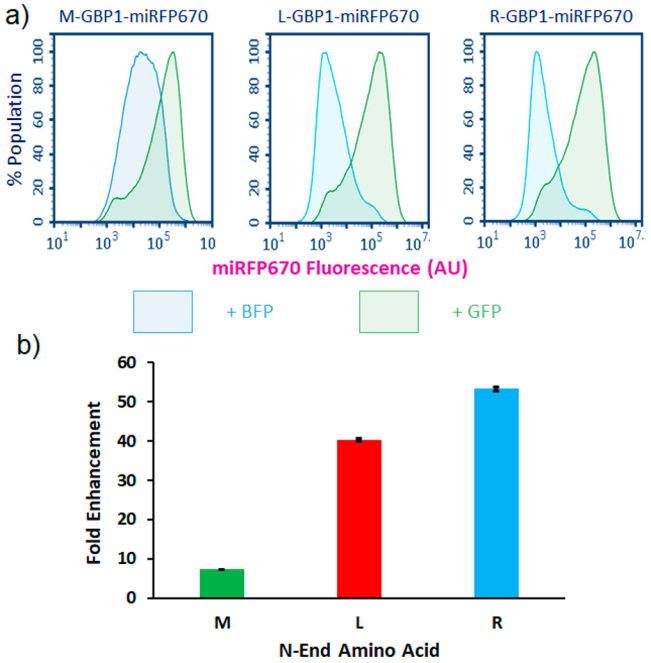

Figure 6. Rescuing protein by blocking N-end rule-mediated degradation. (a) When BFP is coexpressed, miRFP670 rescue does not occur, and the residual fluorescence levels scale well with the reported half-lives of proteins with the respective N-terminal amino acids. However, coexpression of GFP resulted in a significant increase in miRFP670 fluorescence levels. Furthermore, fluorescence levels of rescued protein are comparable regardless of which N-terminal amino acid is used. (b) The fold enhancement measured for each N-terminal amino acid is plotted as a function of the median miRFP670 fluorescence when coexpressed with GFP divided by the median when coexpressed with BFP (background fluorescence). Each N-terminal amino acid noted some enhancement, with Arg measuring more than 50× enhancement. Error bars represent a 95% confidence interval.

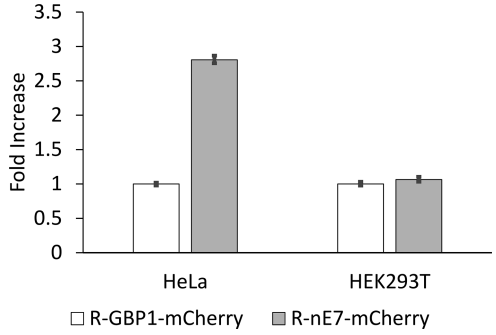

Figure 7. Detecting an endogenous cancer marker using CPR. HeLa cells are cancerous as a consequence of infection with HPV. These viral proteins provide a specific marker for HeLa cells that can be detected by nE7 nanobody (left). HEK293T cells do not contain this marker, and therefore no statistically significant difference is observed. For both cell types, median fluorescence is normalized to R-GBP1-mCherry fluorescence (background) and plotted as a fold increase above the normalized median. Error bars represent 95% confidence intervals.

positive cells. HPV is a known oncovirus that mainly relies on two proteins to induce carcinogenesis in cervical cells: E6, a major suppressor of apoptosis, and E7, a driver of the cell cycle.[41−43] Using E7 as a HPV marker, we exploited nE7, a nanobody that detects E7,[44] to generate Ub:R-nE7-mCherry to execute CPR. We transfected this construct and the control Ub:R-GBP1-mCherry into both HPV-positive HeLa cells and HPV-negative HEK293T cells. The HEK293T cells showed low levels of mCherry fluorescence regardless of which nanobody was used to perform CPR (Figure 7). However, while GBP1 resulted in low levels of mCherry in the HeLa cells, nE7 resulted in a roughly 3-fold increase in mCherry, demonstrating that CPR is capable of detecting even low levels of a cellular target protein.

We report here a new synthetic biology framework to elicit CPR based on proteomic information. To our knowledge, this is the first report that allows for the rescue of a target protein from degradation using a second protein as a masking agent. Although the initial feasibility was demonstrated using the SpyTag/SpyCatcher bioconjugation pair, even noncovalent interactions can be used to achieve similar rescue efficiencies. The modularity of the design allows the addition of a UbL proteasome-targeting domain to eliminate background while still allowing rescue of a POI. The use of nanobodies as a small sensing domain removes the limit on the potential target pool and creates a new synthetic biology framework by allowing endogenous cellular proteins to decide the fate of a POI. We demonstrated this feasibility by detecting E7, a protein unique to HPV-positive cells. The availability of DDs with a wide range of degradation kinetics, including the N-end rule, offers the possibility to elicit rescue by an endogenous protein in a threshold-dependent manner. By combining different DDs and sensing domains, it may be possible to generate more complex, multi-input protein logic gates to help further differentiate between disease and healthy cells for therapeutic applications.

METHODS

Plasmid Construction. All constructs were prepared using standard molecular cloning techniques and cloned into pcDNA3.1(+) (Invitrogen). All oligonucleotides were ordered from Integrated DNA Technology (Coralville, IA) and purified via standard desalting. All enzymes were purchased from New England Biolabs (Ipswich, IA) and used per the manufacturer's protocol with the provided buffers. All overlapping oligos were first 5′ phosphorylated with T4 polynucleotide kinase (PNK) treatment, and then were heat denatured and slow cooled to allow for proper hybridization before ligation.

mCherry:T2A:YFP-cODC1-SpyTag. YFP was PCR amplified and double digested with *AflII* and *XhoI*. The DNA sequences for oCDC1-SpyTag were ordered as overlapping oligonucleotides as ultrameres with appropriate overhangs to make them complementary to *XhoI* and *ApaI*. The vector pcDNA3.1(+) was double digested with *AflII* and *ApaI* to generate the backbone, and YFP and cODC1-SpyTag were ligated simultaneously using T4 DNA Ligase per the manufacturer's protocol to generate YFP-cODC1-SpyTag. Finally, mCherry was PCR amplified with a reverse primer that included the T2A region in the nonoverlapping region, and this product was double digested with *NheI* and *AflII*. YFP-cODC1-SpyTag was double digested with *NheI* and *AflII*, and mCherry:T2A was ligated, generated mCherry:T2A:YFP-cODC1-SpyTag.

SpyCatcher-mCherry:T2A:YFP-cODC1-SpyTag. SpyCatcher was codon optimized and ordered as a gBlock gene fragment. SpyCatcher was then PCR amplified and double digested with *NheI* and *Eco*RI. mCherry:T2A was PCR amplified with the same reverse primer as above, but the

https://dx.doi.org/10.1021/acssynbio.0c00367
ACS Synth. Biol. 2020, 9, 2639−2647

forward primer provided an N-terminal *Eco*RI site, and this product was double digested with *Eco*RI and *AflII*. mCherry:T2A:YFP-cODC1-SpyTag was double digested with *NheI* and *AflII* to remove mCherry:T2A and generate the backbone into which SpyCatcher and mCherry:T2A were simultaneously ligated, generating SpyCatcher-mCherry:-T2A:YFP-cODC1-SpyTag.

miRFP670 Constructs. miRFP670 was PCR amplified and double digested with *NheI* and *Hin*dIII. The T2A polycistronic site was ordered as two overlapping oligonucleotides with overhangs to provide *Hin*dIII and *AflII* complementary sites. mCherry:T2A:YFP-cODC1-SpyTag was double digested with *NheI* and *AflII* to remove mCherry:T2A. miRFP670 and T2A were simultaneously ligated with the backbone to generate miRFP670:T2A:YFP-cODC1-SpyTag. Next, miRFP670 was PCR amplified with overhangs providing *Eco*RI and *Hin*dIII sites, and the product was double digested at those sites. The human codon optimized SpyCatcher was PCR amplified and double digested with *NheI* and *Eco*RI as described above. miRFP670:T2A:YFP-cODC1-SpyTag was double digested with *NheI* and *Hin*dIII to remove miRFP670, and SpyCatcher and miRFP670 was simultaneously ligated into the backbone, generating SpyCatcher-miRFP670:T2A:YFP-cODC1-SpyTag. Finally, SH3 was PCR amplified. SH3 and SpyCatcher-miRFP670:T2A:YFP-cODC1-SpyTag were double digested with *NheI* and *Eco*RI to remove SpyCatcher, and SH3 was ligated to generate SH3-miRFP670:T2A:YFP-cODC1-SpyTa*SH3* and *SH3Lig constructs*. SH3 was PCR amplified and double digested with *NheI* and *Eco*RI. SH3Lig was ordered as a pair of overlapping oligonucleotides with overhangs providing for *XbaI* and *ApaI* complementation sites. Previous plasmids could be double digested with *NheI* and *Eco*RI (to install SH3) or *XbaI* and *ApaI* (to install SH3Lig) to generate SpyCatcher-mCherry:T2A:YFP-cODC1-SH3Lig, SH3-mCherry:T2A:YFP-cODC1-SpyTag, or SH3-mCherry:T2A:YFP-cODC1-SH3Lig.

miRFP670-cODC1-SpyTag-GBP1. SpyTag was ordered as a pair of overlapping oligonucleotides providing overhangs with *XbaI* and *Bam*HI. The GFP Nanobody (GBP1), *aka* GFP Binding Protein 1 (GBP1), was PCR amplified and double digested with *Bam*HI and *ApaI*. mCherry:T2A:YFP-cODC1-SpyTag was double digested with *XbaI ApaI* to remove SpyTag, and SpyTag and GBP1 were simultaneously ligated into the backbone generating mCherry:T2A:YFP-cODC1-SpyTag-GBP1. Next, miRFP670 was PCR amplified and double digested with *AflII* and *XhoI*, and mCherry:-T2A:YFP-cODC1-SpyTag-GBP1 was double digested with *XhoI* and *ApaI* in order to purify cODC1-SpyTag-GBP1. pcDNA3.1(+) was double digested with *AflII* and *ApaI*, and miRFP670 and cODC1-SpyTag-GBP1 were simultaneously ligated into the vector to generate miRFP670-cODC1-SpyTag-GBP1.

yCD Constructs. BFP was PCR amplified and double digested with *NheI* and *ClaI*. A T2A site was ordered as overlapping ultramers with overhangs providing *ClaI* and *AflII* complementation sites. mCherry:T2A:YFP-cODC1-SpyTag-GBP1 was double digested with *NheI* and *AflII* to remove mCherry:T2A. BFP and T2A were simultaneously ligated into the cut vector to generate BFP:T2A:YFP-cODC1-SpyTag-GBP1. A second BFP was PCR amplified and double digested with *Eco*RI and *ClaI*. SH3 was again PCR amplified similar to above and double digested with *NheI* and *Eco*RI. BFP:T2A:YFP-cODC1-SpyTag-GBP1 was then double digested with *NheI* and *ClaI*, and SH3 and BFP were ligated to generate SH3-BFP:T2A:YFP-cODC1-SpyTag-GBP1. yCD was PCR amplified and double digested with *AflII* and *Xho*I. SH3-BFP:T2A:YFP-cODC1-SpyTag-GBP1 was also double digested with *AflII* and *XhoI* to remove YFP, and yCD was ligated in its place generating SH3-BFP:T2A:YFP-cODC1-SpyTag-GBP1. To generate the rescuing construct, EGFP was PCR amplified and double digested with *NheI* and *Eco*RI. The previous construct was double digested with the same enzymes to remove SH3, and GFP was ligated in its place generating GFP-BFP:T2A:YFP-cODC1-SpyTag-GBP1.

UbL Constructs. A single copy of the UbL domain was PCR amplified and double digested with *AflII* and *ClaI*. YFP was also PCR amplified and double digested with *ClaI* and *XhoI*. Both mCherry:T2A:YFP-cODC1-SpyTag and SpyCatcher-mCherry:T2A:YFP-cODC1-SpyTag were double digested with *AflII* and *XhoI* to remove YFP, and UbL and YFP were simultaneously ligated into the cut vector to generate mCherry:T2A:UbL-YFP-cODC1-SpyTag and SpyCatcher-mCherry:T2A:UbL-YFP-cODC1-SpyTag, respectively.

N-End Rule Constructs. Ub-R-GFP was a gift from Nico Dantuma (Addgene plasmid no. 11939; http://n2t.net/addgene:11939; RRID:Addgene_11939). Site directed mutagenesis was performed to generated Ub M-GFP and Ub-L-GFP using Q5 Hot Start High-Fidelity Polymerase New England Biolabs (Ipswich, IA) according to the manufacture's protocol. *Kpn*I and *Bam*HI restriction sites were introduced via mutagenesis between the N-terminal amino acid and GFP, and GBP1 was inserted into these sites. Finally, GFP was excised using *Bam*HI and NotI, and miRFP670 was ligated in its place to generate Ub X-GBP1-miRFP670.

LaM4 Constructs. To generate EGFP-cODC1-LaM4, EGFP was PCR amplified to include AflII and XhoI restriction sites. miRFP670-cODC1-GBP1 was digested with AflII and XhoI, and EGFP was ligated to generate EGFP-cODC1-GBP1. GBP1 was excised using *Bam*HI and ApaI, and LaM4 was ligated in its place. N-End rule constructs were generated by excising GBP1 from Ub X-GBP1-EGFP using *Kpn*I and *Bam*HI; LaM4 was ordered as a gene fragment and PCR amplified to include the same restriction sites, and the ligation product yielded Ub X-LaM4-EGFP.

nE7 Constructs. Ub R-GBP1-miRFP670 was digested with *Kpn*I and *Bam*HI. The nE7 nanobody was ordered as a gene fragment from IDT, PCR amplified to include *Kpn*I and *Bam*HI restriction sites, and ligated into the vector. This subclone was subsequently digested with AgeI and NotI, and mCherry was PCR amplified and cloned into place to yield Ub R-nE7-mCherry. To generate the control construct, Ub R-GBP1-miRFP670 was digested with AgeI and NotI, and mCherry was PCR amplified and ligated into the vector to yield Ub R-GBP1-mCherry.

Cell Culture. HeLa cells were maintained in T150 tissue culture flasks (Thermo Fisher) in complete media, that is, Minimum Essential Media (MEM, Cellgro) supplemented with 10% fetal bovine serum (FBS, Corning), 10 U mL^{-1} penicillin (HyClone), and 10 U mL^{-1} streptomycin (HyClone) at 37 °C and 5% CO_2. Cell passaging occurred upon reaching confluency in the flask by treating with 0.05% trypsin-EDTA for 4 min at 37 °C and 5% CO_2. Cells were pelleted at 500*g* for 10 min, resuspended in 5 mL of complete media, and counted. HeLa cells were seeded in 12-well plates at 175 000 cells/well and 6-well plates at 750 000 cells/well. HEK293T cells were seeded in 6-well plates at 250 000 cells/well.

https://dx.doi.org/10.1021/acssynbio.0c00367
ACS Synth. Biol. 2020, 9, 2639−2647

Transfection. Plasmid DNA was prepared using Zymo-PURE Plasmid Midiprep Kit (Zymo Research) according to the manufacture's protocol. One day after seeding, transfection was achieved with Lipofectamine 3000 (Invitrogen) using 1 μg of total plasmid DNA per well for 6-well plates and 2.5 μg of total plasmid DNA for 12-well plates in complete media and following the manufacture's protocol. Where more than one plasmid was transfected, the total DNA was split evenly among all plasmids unless otherwise noted.

Fluorescent Microscopy and Image Analysis. All images were captured using an Observer Z.1 Inverted Microscope (Zeiss) with GFP, mCherry, BFP, or Cy5 filter cube sets (Chroma). For image analysis, five images were captured in each well. Image analysis was conducted using the "Measure" analysis in ImageJ with the threshold set at 10−255. Error bars on all plots represent the 95% confidence interval.

Western Blotting. Following imaging, cells were incubated in ice-cold lysis buffer (50 mM Tris, 150 mM NaCl, 1% Triton X-100, pH 8.0) on ice for 20 min with protease inhibitor cocktail (Calbiochem). Cells were then removed from the plate with a cell scrapper (Genemate), and the lysate was clarified in a precooled centrifuge at 12 000 rpm for 10 min at 4 °C. Total protein concentrations were normalized through a Bradford assay (Bio-Rad) with a BSA standard. Fifteen micrograms of lysate was mixed with a 5× loading buffer and separated by 10% SDS-PAGE before being transferred to a nitrocellulose membrane (Bio-Rad).

Western blots were blocked in TBST (20 mM Tris, 500 mM NaCl, 0.05% Tween-20, pH 8.0) containing 5% nonfat milk overnight at room temperature with gentle shaking. Membranes were washed twice in TBST and incubated for 3 h in anti-GFP (1:5000 dilution, Covance) or anti-mCherry (1:2000 dilution, Novus) in TBS. The blots were then washed twice in TBST and incubated with horseradish peroxidase (HRP)-conjugated secondary antibody (GenScript) for 2 h in TBST. The blots were washed three times in TBST and developed using ECL reagents (GE) according to the manufactures protocol. Band intensities were quantified using ImageJ gel analysis tools.

Flow Cytometry. Most flow cytometry was conducted on the Novocyte Benchtop Flow Cytometer (Acea Biosciences, San Diego, CA). Experiments involving mCherry (Ub R-nE7-mCherry and Ub X-LaM4-EGFP rescued with mCherry) were conducted on BD FACSAria Fusion High Speed Cell Sorter (BD Biosciences, San Jose, CA). All flow cytometry experiments involved ≥50 000 transfected cells as determined by forward- and side-scatter profiles of recorded events and fluorescent gating to exclude cells not transfected by at least the rescuing protein for each respective experiment. Cells were prepared for flow cytometry by washing twice in warm PBS. Trypsin treatment was applied for 3 min, and the reaction was quenched by warm media. Cells were collected in microcentrifuge tubes and spun at 0.8 g for 5 min. The supernatant was aspirated, and cells were resuspended in cold PBS. This solution was then passed through a cell strainer into a flow cytometer tube and stored on ice until analysis.

yCD Viability Studies. HeLa cells were seeded as above in 6-well plates and transfected with the appropriate constructs as above. Approximately 1 day post-transfection, wells either received no treatment, 5-FC, or 5-FU for 48 h. Viability was determined using NucRed Dead 647 ReadyProbes Reagent (Thermo Fisher) per the manufacturer's instruction. Fluorescent microscopy was used for analysis as described above.

E7 Detection Studies. HeLa cells and HEK293T cells were seeded as described above. Transfection was conducted for 6 h, and then replaced with normal media. Flow cytometry analysis was conducted 24 h post-transfection as described above.

Statistical Analysis. All the experiments were performed in biological triplicates with at least 5 data points per replicate, and results were expressed as means at a 95% confidence interval (CI). Statistical significance was analyzed using the student t-tests. $P < 0.05$ was considered statistically significant throughout the study.

■ ASSOCIATED CONTENT

Supporting Information

The Supporting Information is available free of charge at https://pubs.acs.org/doi/10.1021/acssynbio.0c00367.

All oligo sequences used in this study; supplemental figures as described in the text (PDF)

■ AUTHOR INFORMATION

Corresponding Author

Wilfred Chen − *Department of Chemical and Biomolecular Engineering, University of Delaware, Newark, Delaware 19716, United States;* orcid.org/0000-0002-6386-6958; Email: wilfred@udel.edu

Author

Andrew S. Gaynor − *Department of Chemical and Biomolecular Engineering, University of Delaware, Newark, Delaware 19716, United States*

Complete contact information is available at: https://pubs.acs.org/10.1021/acssynbio.0c00367

Author Contributions

A.S.G. and W.C. conceived the project. A.S.G. designed experiments, performed the experiments, analyzed the data, and wrote the manuscript. W.C. designed experiments, analyzed the data, and wrote the manuscript. Both authors discussed the results and commented on the manuscript.

Notes

The authors declare no competing financial interest.

■ ACKNOWLEDGMENTS

This work was funded by NSF (CBET1803008 and CBET1510817).

■ ABBREVIATIONS

DD, degradation domain; POI, protein of interest; CPR, conditional protein rescue; MBP, maltose binding protein; GBP1, GFP binding protein 1; yCD, yeast cytosine deaminase; 5-FC, 5-fluorocytosine; 5-FU, 5-fluoruracile; PCE, prodrug converting enzyme

■ REFERENCES

(1) Sigoillot, F. D., and King, R. W. (2011) Vigilance and Validation: Keys to Success in RNAi Screening. *ACS Chem. Biol.* 6 (1), 47−60.

(2) Battle, A., Khan, Z., Wang, S. H., Mitrano, A., Ford, M. J., Pritchard, J. K., and Gilad, Y. (2015) Impact of Regulatory Variation from RNA to Protein. *Science* 347 (6222), 664−667.

(3) Wu, L., Candille, S. I., Choi, Y., Xie, D., Jiang, L., Li-Pook-Than, J., Tang, H., and Snyder, M. (2013) Variation and Genetic Control of Protein Abundance in Humans. *Nature* 499 (7456), 79−82.

(4) Vogel, C., and Marcotte, E. M. (2012) Insights into the Regulation of Protein Abundance from Proteomic and Transcriptomic Analyses. *Nat. Rev. Genet. 13* (4), 227−232.
(5) Li, X., Zhao, X., Fang, Y., Jiang, X., Duong, T., Fan, C., Huang, C. C., and Kain, S. R. (1998) Generation of Destabilized Green Fluorescent Protein as a Transcription Reporter. *J. Biol. Chem. 273* (52), 34970−34975.
(6) Mei, L., Fan, Y., Lv, X., Welsh, D. K., Zhan, C., and Zhang, E. E. (2018) Long-Term in Vivo Recording of Circadian Rhythms in Brains of Freely Moving Mice. *Proc. Natl. Acad. Sci. U. S. A. 115* (16), 4276−4281.
(7) Sjaastad, L. E., Fay, E. J., Fiege, J. K., Macchietto, M. G., Stone, I. A., Markman, M. W., Shen, S., and Langlois, R. A. (2018) Distinct Antiviral Signatures Revealed by the Magnitude and Round of Influenza Virus Replication in Vivo. *Proc. Natl. Acad. Sci. U. S. A. 115* (38), 9610−9615.
(8) Chen, R. P., Gaynor, A. S., and Chen, W. (2019) Synthetic Biology Approaches for Targeted Protein Degradation. *Biotechnol. Adv. 37* (8), 107446.
(9) Chung, H. K., Jacobs, C. L., Huo, Y., Yang, J., Krumm, S. A., Plemper, R. K., Tsien, R. Y., and Lin, M. Z. (2015) Tunable and Reversible Drug Control of Protein Production via a Self-Excising Degron. *Nat. Chem. Biol. 11* (9), 713−720.
(10) Iwamoto, M., Björklund, T., Lundberg, C., Kirik, D., and Wandless, T. J. (2010) A General Chemical Method to Regulate Protein Stability in the Mammalian Central Nervous System. *Chem. Biol. 17* (9), 981−988.
(11) Lau, H. D., Yaegashi, J., Zaro, B. W., and Pratt, M. R. (2010) Precise Control of Protein Concentration in Living Cells. *Angew. Chem., Int. Ed. 49* (45), 8458−8461.
(12) Harper, J. W., Burton, J. L., and Solomon, M. J. (2002) The Anaphase-Promoting Complex: It's Not Just for Mitosis Any More. *Genes Dev. 16* (17), 2179−2206.
(13) Morgan, D. O. (1997) CYCLIN-DEPENDENT KINASES: Engines, Clocks, and Microprocessors. *Annu. Rev. Cell Dev. Biol. 13* (1), 261−291.
(14) Sherr, C. J., and Roberts, J. M. (1999) CDK Inhibitors: Positive and Negative Regulators of G1-Phase Progression. *Genes Dev. 13* (12), 1501−1512.
(15) Shemorry, A., Hwang, C. S., and Varshavsky, A. (2013) Control of Protein Quality and Stoichiometries by N-Terminal Acetylation and the N-End Rule Pathway. *Mol. Cell 50* (4), 540−551.
(16) Zhang, Z., Kulkarni, K., Hanrahan, S. J., Thompson, A. J., and Barford, D. (2010) The APC/C Subunit Cdc16/Cut9 Is a Contiguous Tetratricopeptide Repeat Superhelix with a Homo-Dimer Interface Similar to Cdc27. *EMBO J. 29* (21), 3733−3744.
(17) Oh, J.-H., Hyun, J.-Y., and Varshavsky, A. (2017) Control of Hsp90 Chaperone and Its Clients by N-Terminal Acetylation and the N-End Rule Pathway. *Proc. Natl. Acad. Sci. U. S. A. 114* (22), E4379.
(18) Renicke, C., Schuster, D., Usherenko, S., Essen, L. O., and Taxis, C. (2013) A LOV2 Domain-Based Optogenetic Tool to Control Protein Degradation and Cellular Function. *Chem. Biol. 20* (4), 619−626.
(19) Jungbluth, M., Renicke, C., and Taxis, C. (2010) Targeted Protein Depletion in Saccharomyces Cerevisiae by Activation of a Bidirectional Degron. *BMC Syst. Biol. 4* (1), 176.
(20) Taxis, C., Stier, G., Spadaccini, R., and Knop, M. (2009) Efficient Protein Depletion by Genetically Controlled Deprotection of a Dormant N-Degron. *Mol. Syst. Biol. 5*, 267.
(21) Zakeri, B., Fierer, J. O., Celik, E., Chittock, E. C., Schwarz-Linek, U., Moy, V. T., and Howarth, M. (2012) Peptide Tag Forming a Rapid Covalent Bond to a Protein, through Engineering a Bacterial Adhesin. *Proc. Natl. Acad. Sci. U. S. A. 109* (12), E690−7.
(22) Szymczak, A. L., Workman, C. J., Wang, Y., Vignali, K. M., Dilioglou, S., Vanin, E. F., and Vignali, D. A. A. (2004) Correction of Multi-Gene Deficiency in Vivo Using a Single "self-Cleaving" 2A Peptide-Based Retroviral Vector. *Nat. Biotechnol. 22* (5), 589−594.
(23) Holst, J., Burton, A. R., Vignali, K. M., and Vignali, D. A. A. (2006) Rapid Analysis of T-Cell Selection in Vivo Using T Cell-Receptor Retrogenic Mice. *Nat. Methods 3* (3), 191−197.
(24) Shcherbakova, D. M., Baloban, M., Emelyanov, A. V., Brenowitz, M., Guo, P., and Verkhusha, V. V. (2016) Bright Monomeric Near-Infrared Fluorescent Proteins as Tags and Biosensors for Multiscale Imaging. *Nat. Commun. 7* (1), 12405.
(25) Li, S. S. (2005) Specificity and Versatility of SH3 and Other Proline-Recognition Domains: Structural Basis and Implications for Cellular Signal Transduction. *Biochem. J. 390* (3), 641−653.
(26) Dueber, J. E., Mirsky, E. A., and Lim, W. A. (2007) Engineering Synthetic Signaling Proteins with Ultrasensitive Input/Output Control. *Nat. Biotechnol. 25* (6), 660−662.
(27) Kubala, M. H., Kovtun, O., Alexandrov, K., and Collins, B. M. (2010) Structural and Thermodynamic Analysis of the GFP:GFP-Nanobody Complex. *Protein Sci. 19* (12), 2389−2401.
(28) Saerens, D., Pellis, M., Loris, R., Pardon, E., Dumoulin, M., Matagne, A., Wyns, L., Muyldermans, S., and Conrath, K. (2005) Identification of a Universal VHH Framework to Graft Non-Canonical Antigen-Binding Loops of Camel Single-Domain Antibodies. *J. Mol. Biol. 352* (3), 597−607.
(29) Tang, J. C. Y., Szikra, T., Kozorovitskiy, Y., Teixiera, M., Sabatini, B. L., Roska, B., and Cepko, C. L. (2013) A Nanobody-Based System Using Fluorescent Proteins as Scaffolds for Cell-Specific Gene Manipulation. *Cell 154* (4), 928−939.
(30) Polak, A., Eschenhof, E., Fernex, M., and Scholer, H. J. (2004) Metabolic Studies with 5-Fluorocytosine-6−14C in Mouse, Rat, Rabbit, Dog and Man. *Chemotherapy 22* (3−4), 137−153.
(31) Zhang, J., Kale, V., and Chen, M. (2015) Gene-Directed Enzyme Prodrug Therapy. *AAPS J. 17* (1), 102−110.
(32) Prakash, S., Inobe, T., Hatch, A. J., and Matouschek, A. (2009) Substrate Selection by the Proteasome during Degradation of Protein Complexes. *Nat. Chem. Biol. 5* (1), 29−36.
(33) Stack, J. H., Whitney, M., Rodems, S. M., and Pollok, B. A. (2000) A Ubiquitin-Based Tagging System for Controlled Modulation of Protein Stability. *Nat. Biotechnol. 18* (12), 1298−1302.
(34) Elsasser, S., Gali, R. R., Schwickart, M., Larsen, C. N., Leggett, D. S., Müller, B., Feng, M. T., Tübing, F., Dittmar, G. A. G., and Finley, D. (2002) Proteasome Subunit Rpn1 Binds Ubiquitin-like Protein Domains. *Nat. Cell Biol. 4* (9), 725−730.
(35) Yu, H., Gautam, A. K. S., Wilmington, S. R., Wylie, D., Martinez-Fonts, K., Kago, G., Warburton, M., Chavali, S., Inobe, T., Finkelstein, I. J., Babu, M. M., and Matouschek, A. (2016) Conserved Sequence Preferences Contribute to Substrate Recognition by the Proteasome. *J. Biol. Chem. 291* (28), 14526−14539.
(36) Choi, W. S., Jeong, B.-C., Joo, Y. J., Lee, M.-R., Kim, J., Eck, M. J., and Song, H. K. (2010) Structural Basis for the Recognition of N-End Rule Substrates by the UBR Box of Ubiquitin Ligases. *Nat. Struct. Mol. Biol. 17* (10), 1175−1181.
(37) Matta-Camacho, E., Kozlov, G., Li, F. F., and Gehring, K. (2010) Structural Basis of Substrate Recognition and Specificity in the N-End Rule Pathway. *Nat. Struct. Mol. Biol. 17* (10), 1182−1187.
(38) Bachmair, A., Finley, D., and Varshavsky, A. (1986) In Vivo Half-Life of a Protein Is a Function of Its Amino-Terminal Residue. *Science (Washington, DC, U. S.) 234* (4773), 179−186.
(39) Gonda, D. K., Bachmair, A., Wunning, I., Tobias, J. W., Lane, W. S., and Varshavsky, A. (1989) Universality and Stucture of the N-End Rule. *J. Biol. Chem. 264* (28), 16700−16712.
(40) Fridy, P. C., Li, Y., Keegan, S., Thompson, M. K., Nudelman, I., Scheid, J. F., Oeffinger, M., Nussenzweig, M. C., Fenyö, D., Chait, B. T., and Rout, M. P. (2014) A Robust Pipeline for Rapid Production of Versatile Nanobody Repertoires. *Nat. Methods 11* (12), 1253−1260.
(41) Jansma, A. L., Martinez-Yamout, M. A., Liao, R., Sun, P., Dyson, H. J., and Wright, P. E. (2014) The High-Risk HPV16 E7 Oncoprotein Mediates Interaction between the Transcriptional Coactivator CBP and the Retinoblastoma Protein PRb. *J. Mol. Biol. 426* (24), 4030−4048.
(42) Senba, M., and Mori, N. (2012) Mechanisms of Virus Immune Evasion Lead to Development from Chronic Inflammation to Cancer

https://dx.doi.org/10.1021/acssynbio.0c00367
ACS Synth. Biol. 2020, 9, 2639−2647

Formation Associated with Human Papillomavirus Infection. *Oncol. Rev.* 6 (2), No. e17.
(43) Moody, C. A., and Laimins, L. A. (2010) Human Papillomavirus Oncoproteins: Pathways to Transformation. *Nat. Rev. Cancer 10*, 550−560.
(44) Li, S., Zhang, W., Jiang, K., Shan, H., Shi, M., Chen, B., and Hua, Z. (2019) Nanobody against the E7 Oncoprotein of Human Papillomavirus 16. *Mol. Immunol. 109*, 12−19.

https://dx.doi.org/10.1021/acssynbio.0c00367
ACS Synth. Biol. 2020, 9, 2639−2647